NANO LETTERS

Letter

pubs.acs.org/NanoLett

Morphing a Plasmonic Nanodisk into a Nanotriangle

Franz P. Schmidt,[†,‡] Harald Ditlbacher,[†] Ferdinand Hofer,[‡] Joachim R. Krenn,[†] and Ulrich Hohenester*[,†]

[†]Institut für Physik, Karl–Franzens–Universität Graz, Universitätsplatz 5, 8010 Graz, Austria

[‡]Institute for Electron Microscopy and Nanoanalysis (FELMI), Graz University of Technology, 8010 Graz, Austria

ABSTRACT: We morph a silver nanodisk into a nanotriangle by producing a series of nanoparticles with electron beam lithography. Using electron energy loss spectroscopy (EELS), we map out the plasmonic eigenmodes and trace the evolution of edge and film modes during morphing. Our results suggest that disk modes, characterized by angular order, can serve as a suitable basis for other nanoparticle geometries and are subject to resonance energy shifts and splittings, as well as to hybridization upon morphing. Similar to the linear combination of atomic orbitals (LCAO) in quantum chemistry, we introduce a *linear combination of plasmonic eigenmodes* to describe plasmon modes in different geometries, hereby extending the successful hybridization model of plasmonics.

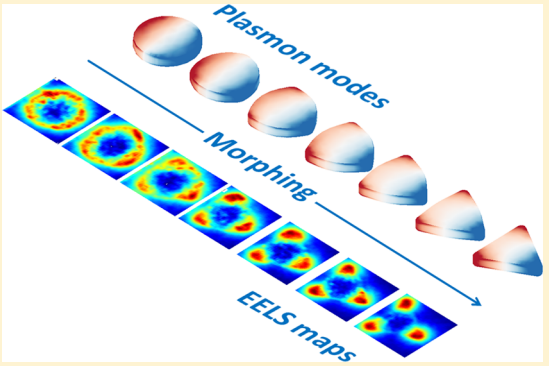

KEYWORDS: *Plasmonics, nanoparticles, electron beam lithography, electron energy loss spectroscopy, hybridization*

Electron energy loss spectroscopy (EELS) has recently emerged as an ideal measurement device for plasmonic nanoparticles.[1] Electrons with kinetic energies of hundreds of keV pass by or penetrate through a metallic nanoparticle and excite surface plasmons (SP). By spectroscopically analyzing the energy loss one obtains detailed information about the SP resonances, and by raster-scanning the electron beam over the nanoparticle one can map out the SP field distributions with nanometer resolution, as first demonstrated for nanospheres,[2] nanorods,[3] and nanotriangles.[4] In the last couple of years this technique has been extensively used for the study of various plasmonic nanosystems.[5]

Despite the vast information that has been obtained from such EELS measurements, there are few theoretical concepts suited for a simple and intuitive interpretation of the acquired data, and one is often bound to full numerical simulations.[1,5] Noticeable exceptions are the celebrated hybridization model for plasmonic nanoparticles,[6] which describes SP resonances of coupled nanoparticles as a "hybridization" of elementary plasmons supported by nanostructures of elementary geometries, and the SP ordering scheme for flat nanoparticles, such as nanoplatelets and particles produced with electron beam lithography. In the latter scheme, the SP modes are categorized as film-like excitations, reminiscent of SPs in planar structures, and edge-like modes, which are confined to the nanoparticle edges.[7−10]

Within the "flatland world" of quasi two-dimensional nanoparticles, nanodisks play a distinguished role since the cylinder symmetry leads to conservation of angular momentum, and the SP excitations can be characterized in terms of angular mode orders.[11] This allows for an intuitive ordering of the SP film and edge modes based on solely symmetry.[9,10] Similar to quantum physics, where atomic orbitals with full rotational symmetry are successfully employed for the description of molecular and solid-state wave functions with broken symmetry, one might wonder whether the nanodisk SP modes with full cylinder symmetry might serve as a basis for modes in different geometries, such as nanotriangles.[4,7,8,12]

In this paper we morph a nanodisk into a nanotriangle, by producing with electron-beam lithography a series of nanoparticles in between these two geometries, and employ EELS to track the plasmon peaks during the morphing process. Supplementary simulation results are in good agreement with our experimental findings. Using a plasmon eigenmode expansion within the quasistatic approximation, we devise a perturbation approach that employs the nanodisk eigenmodes as a basis for describing the nanotriangle modes, which allows us to intuitively interpret our EELS results. Similar to the linear combination of atomic orbitals in quantum chemistry, we introduce a *linear combination of plasmonic eigenmodes* to describe plasmon modes in different geometries, where geometric confinement and symmetry breaking lead to peak shifts, splitting of degenerate eigenmodes, and hybridization of film and edge modes. We demonstrate our hybridization description for a few illustrative examples.

Electron beam lithography in a RAITH e-line system was applied to design silver nanostructures of 30 nm thickness on a 15 nm thick Si_3N_4 membrane. A nanodisk with a diameter of approximately 300 nm was stepwise morphed into a nanotriangle, while the circumference was kept constant. EELS was employed in a scanning transmission electron microscope (FEI Tecnai F20) with a monochromated 200 keV electron beam of

Received: May 30, 2014
Revised: June 30, 2014
Published: July 7, 2014

   dx.doi.org/10.1021/nl502027r | *Nano Lett.* 2014, 14, 4810−4815

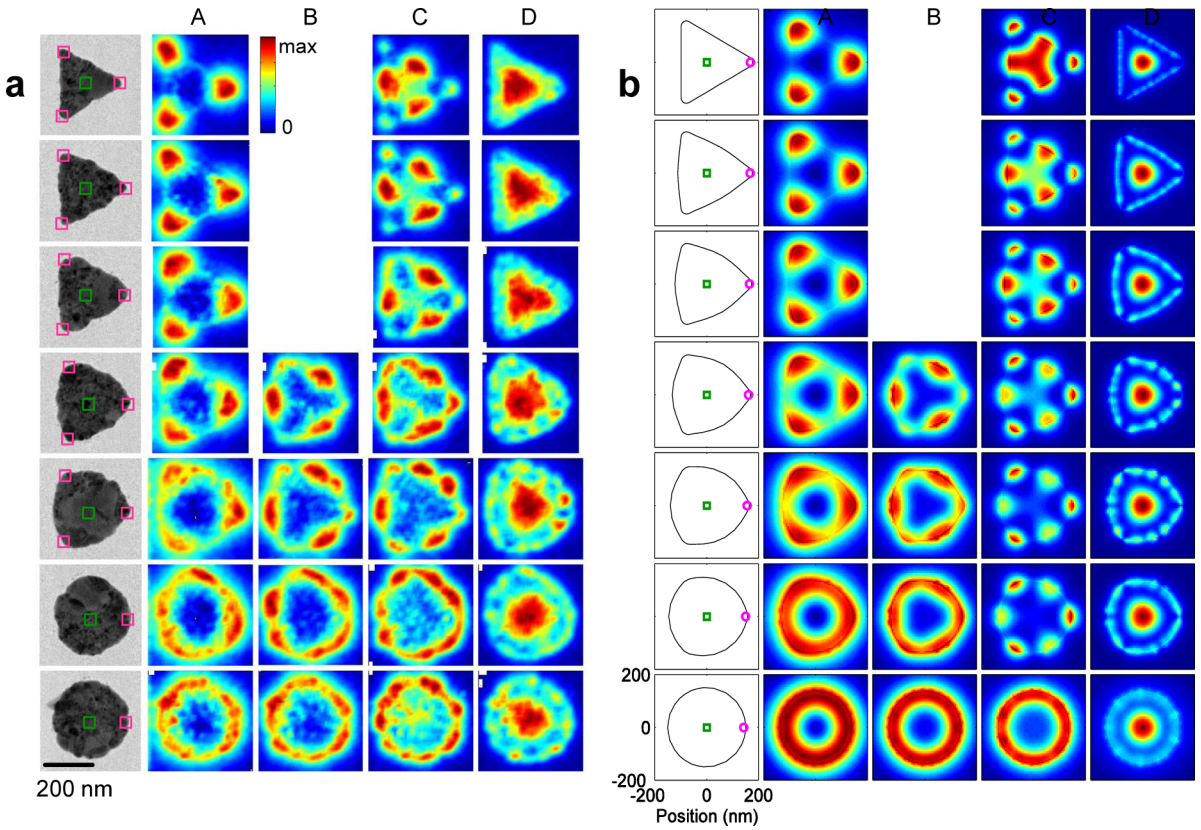

Figure 1. (a) Measured and (b) simulated EELS maps for a morphing from a silver nanodisk (bottom) into a nanotriangle (top). The leftmost column shows TEM images of the lithographically fabricated nanoparticles. Boxes indicate the areas where the EEL spectra shown in Figure 2 are recorded, with averaging of spectra from same-color boxes. The other panels show the evolution of the (A) dipole, (B) quadrupole, (C) hexapole, and (D) breathing mode during morphing. The maps are plotted at the respective peak maxima shown in Figure 2.

130 meV energy spread (full-width-at-half-maximum). EEL spectra were recorded with an energy dispersion of 0.01 eV/channel in a high resolution Gatan Imaging Filter[13] equipped with a 2048 × 2048 pixel CCD camera.

The leftmost column in Figure 1 shows TEM images of the lithographically fabricated nanoparticles, illustrating the morphing of a disk (bottom) into a triangle (top). Panels A–D show EELS maps of these particles at four different mode energies, which will be discussed in more detail below. Spectra were recorded at the corner and center positions of the nanoparticles, indicated by the magenta and green boxes, and are shown in Figure 2. As for the corner position of the nanodisk (bottom of Figure 2a), we can assign the three most prominent peaks of lowest energy to the (A) dipole, (B) quadrupole, and (C) hexapole edge modes, in accordance to ref 9. The first prominent peak at the disk center, shown at the bottom of Figure 2b, is assigned to the (D) breathing mode,[9] a film mode where charge oscillates in the radial direction.

When the disk is morphed into a triangle, the dipole peak A gains intensity. A comparison with the EELS maps shown in Figure 1a reveals that the mode becomes localized at the disk corners. The quadrupole peak B gradually loses intensity and can finally no longer be identified in the spectra. In contrast, the hexapole peak C shifts to lower energies and finally becomes the second peak in the nanotriangle spectrum.[4] We tentatively assign this behavior of peaks B and C to symmetry breaking during morphing: the quadrupole peak with 4-fold symmetry is not commensurable with the triangle geometry and is pushed to higher energies, whereas the hexapole peak with 6-fold symmetry fits to the triangle geometry and is shifted to lower energies. In the final mode pattern, opposite charges reside at the corners and edges of the nanotriangle. The breathing mode D in Figure 2b is pushed to higher energies, probably as an effect of the stronger localization on the triangle (see panel D of Figure 1a). Even more striking, the blueshift of peak D in Figure 2b is accompanied by an intensity increase in the triangle center of the hexapole mode C. This suggests a kind of hybridization, where modes C and D couple and part of the oscillator strength in the nanoparticle center is transferred from the film mode D to the edge mode C.

We additionally performed simulations using the MNPBEM toolbox[14] (see Methods for details). Figure 1b shows the simulated EELS maps, based on the solutions of the full Maxwell equations, which are in good agreement with experiment throughout. The thin lines in Figure 2 report the EEL spectra at the nanoparticle (a) corners and (b) centers. For the simulated spectra in Figure 2 we use an additional broadening of 0.15 eV to account for the finite spectral resolution of our experiments. The peak positions between the experimental and simulation results differ by at most 0.1 eV, a small value which we ascribe to small differences in particle shape, including the grainy surface of the lithographically fabricated particles, and a probably somewhat different silver dielectric function.[15] The peak intensities agree well for the disk center but somewhat deviate at the particle corners, see respectively panels (b) and (a) of Figure 2, probably because of irregularities of the lithographically fabricated nanoparticles. Nevertheless, our simulations show in accordance to experi-

dx.doi.org/10.1021/nl502027r | Nano Lett. 2014, 14, 4810–4815

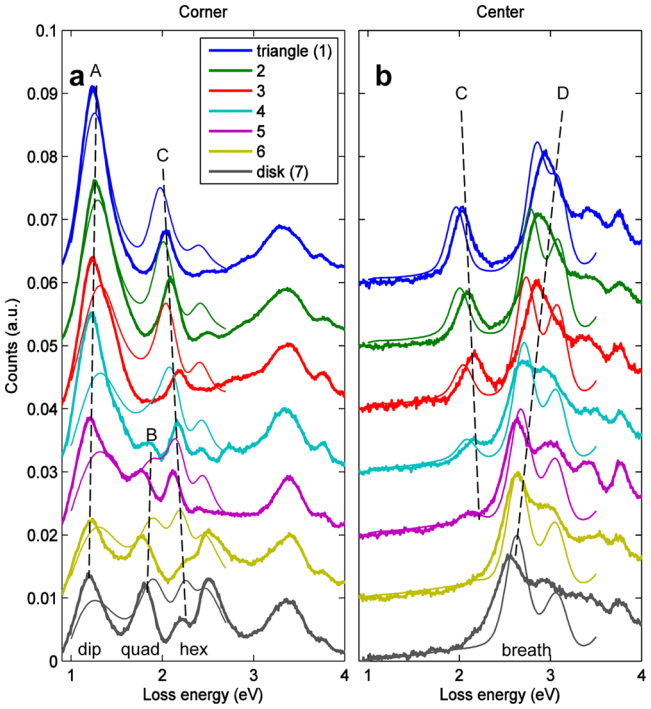

Figure 2. EEL spectra measured at the (a) corner and (b) center positions, indicated in Figure 1a, during the morphing process from a nanodisk (bottom) into a nanotriangle (top). The spectra are offset for clarity. The thin lines report simulation results. The labeled peaks can be assigned to the (A) dipole, (B) quadrupole, and (C) hexapole edge modes, as well as to the film-like (D) breathing mode.

ment: a localization of the dipole mode A at the triangle corners; a slight blueshift and disappearance of the quadrupole peak B; a redshift of the hexapole mode C, which finally becomes the second peak in the triangle spectrum; and a blueshift of the breathing mode D, which is accompanied by an intensity increase of the hexapole mode C in the triangle center.

In the following, we devise a perturbation approach which employs the nanodisk eigenmodes as a basis for describing modes in different geometries. This will allow for an intuitive interpretation of our EELS results and will form the basis for our plasmonic hybridization model. We first introduce plasmonic eigenmodes[1,16−18] and then submit these modes to a perturbation scheme where the deviation of the particle geometry from a disk is treated as the "perturbation".

Within the framework of the quasistatic approximation, suitable for small nanoparticles where retardation effects can be ignored but the full frequency dependence of the dielectric functions is retained, and for the external potential $\phi_{ext}(\mathbf{r})$ of the electron beam the surface charges $\sigma(\mathbf{s})$ at the particle boundary ∂V are computed from[1,18]

$$\Lambda(\omega)\sigma(\mathbf{s}) + \oint_{\partial V} \frac{\partial G(\mathbf{s}, \mathbf{s}')}{\partial n}\sigma(\mathbf{s}')\, da' = -\frac{\partial \phi_{ext}(\mathbf{s})}{\partial n} \qquad (1)$$

Here $G(\mathbf{s}, \mathbf{s}')$ is the Green function connecting positions $\mathbf{s}$ and $\mathbf{s}'$ at the particle boundary, and $\partial/\partial n$ denotes the derivative in the direction of the outer surface normal. The nice thing about eq 1 is that the first term on the left-hand side only depends on the material properties $\Lambda(\omega) = 2\pi[1 + \varepsilon(\omega)]/[1 - \varepsilon(\omega)]$, where $\varepsilon(\omega)$ is the metal dielectric function, whereas the second term only depends on the geometry of the nanoparticle. This allows us to introduce *plasmonic eigenmodes* defined through[16−19]

$$\oint_{\partial V} \frac{\partial G(\mathbf{s}, \mathbf{s}')}{\partial n}\sigma_k(\mathbf{s}')\, da' = \lambda_k \sigma_k(\mathbf{s}) \qquad (2)$$

Here λ_k is the k'th eigenvalue, and $\sigma_k(\mathbf{s})$ is the corresponding eigenfunction. The plasmonic eigenmode energies $E_k = \hbar\omega_k$ can then be obtained from $\mathcal{R}e[\Lambda(\omega_k) + \lambda_k] = 0$.

The gray solid lines in Figure 3a show the plasmon energies for different modes and for the particle morphing from a disk

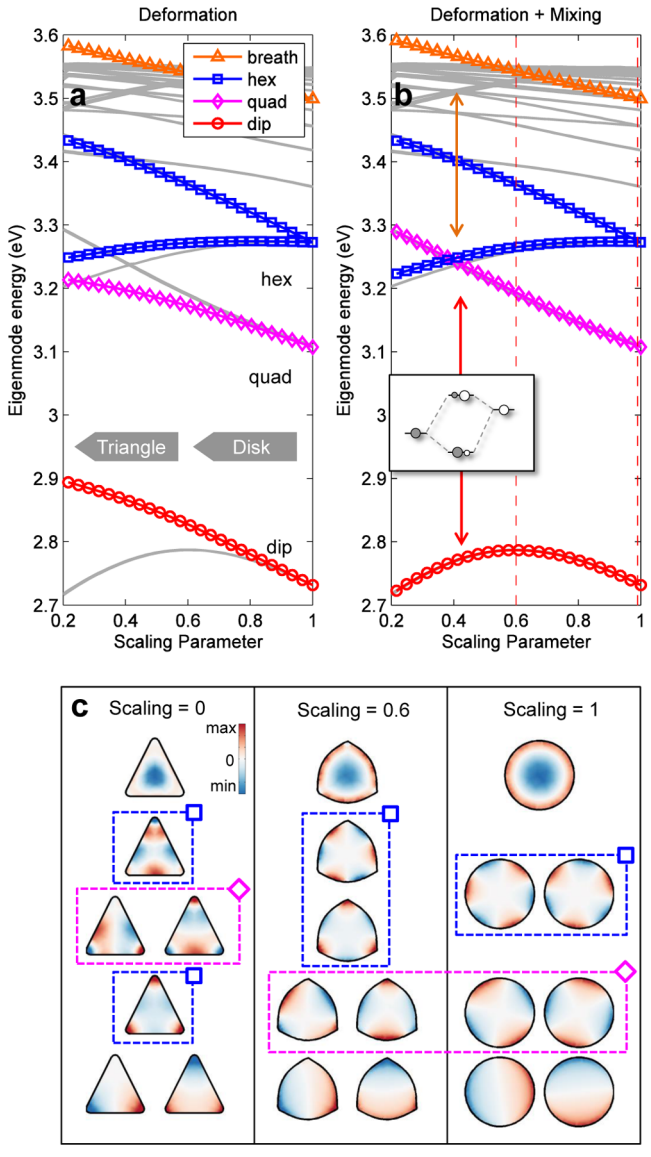

Figure 3. Plasmonic eigenmodes for morphing from a nanodisk (scaling parameter 1, diameter-to-height ratio of 6:1) into a nanotriangle (scaling parameter 0, see Methods for definition of scaling parameter), as computed within the quasistatic approach. The gray lines report the exact eigenmode energies. The symbols in panel (a) show the energies computed from the perturbation approach of eq 3. In panel (b) we allow for an additional coupling between the dipole and quadrupole edge modes, as well as the hexapole edge mode and the filmlike breathing mode. Panel (c) reports the eigenfunctions $\sigma_k(\mathbf{s})$ for different scaling parameters, and for the dipole mode (lowest row), quadrupole mode (magenta box, diamonds), hexapole mode (blue box, squares), and breathing mode (highest row).

dx.doi.org/10.1021/nl502027r | Nano Lett. 2014, 14, 4810−4815

(right) to a triangle (left). In addition to the lowest modes, which can be assigned to the usual dipole, quadrupole, hexapole, and breathing modes, we additionally plot the energies of the other multipolar edge and film modes which will not be further discussed below. Panel (c) reports a few selected eigenfunctions $\sigma_k(\mathbf{s})$. We find that the quadrupole mode is pushed up in energy, whereas the degenerate hexapole mode splits, and the low-energy mode finally becomes the second mode of the triangle. In addition, the breathing mode goes up in energy.

While all these results obtained within the quasistatic framework are qualitatively in agreement with our EELS findings, it is not obvious how to intuitively interpret them. In what follows, we use a perturbation approach[20] in order to use the disk eigenmodes as a basis for describing modes in different particle geometries. This approach is similar to perturbation theory in quantum mechanics,[21] where the eigenenergies E_k^0 and functions $|\phi_k^0\rangle$ of a Hamiltonian $\hat{H}_0$ are used to compute the approximate eigenenergies $E_k \approx E_k^0 + \langle\phi_k^0|\hat{H}'|\phi_k^0\rangle$ in the presence of a "perturbation", described by the Hamiltonian $\hat{H}'$. Such a perturbation approach is for instance employed in quantum chemistry, where one starts from the "unperturbed" atomic orbitals and then performs a linear combination of atomic orbitals (LCAO) to get the approximate molecular energies and states.

In the plasmonic case the matrix $\partial G/\partial n \equiv F$ is not symmetric, and we thus have to introduce in addition to the right plasmonic eigenfunctions $\sigma_k(\mathbf{s})$ also the left eigenfunctions $\tilde{\sigma}_k(\mathbf{s})$, which are biorthogonal and have the same eigenvalues λ_k.[16,18,20] Apart from this complication, the perturbation approach is completely similar to that of quantum mechanics. Let λ_k^0 and σ_k^0 ($\tilde{\sigma}_k^0$) denote the eigenvalues and right (left) eigenfunctions of the "unperturbed" disk. We next compute the Green function matrices F_0 and F for the disk and a different particle geometry, respectively, and treat the difference $F' = F - F_0$ as a "perturbation". The eigenvalues λ_k for the "perturbed" particle geometry are then computed according to

$$\lambda_k \approx \lambda_k^0 + \oint_{\partial V} \tilde{\sigma}_k^0(\mathbf{s})\, F'(\mathbf{s},\mathbf{s}')\, \sigma_k^0(\mathbf{s})\, \mathrm{d}a' \equiv \lambda_k^0 + F'_{kk} \tag{3}$$

The degenerate edge modes of the nanodisk have to be treated differently. Let a and b denote two degenerate modes, such as the dipole or quadrupole edge modes with angular dependences of $e^{\pm i\varphi}$ or $e^{\pm 2i\varphi}$, respectively. We then obtain the two eigenvalues through diagonalization of the matrix

$$\begin{pmatrix} \lambda_a^0 + F'_{aa} & F'_{ab} \\ F'_{ba} & \lambda_b^0 + F'_{bb} \end{pmatrix} \tag{4}$$

The symbols in Figure 3a show the eigenenergies computed from our perturbation approach of eqs 3 and 4. The approximate plasmonic mode energies are throughout in agreements with the exact energies E_k, at least qualitatively, even for geometries where the particle deformation can hardly be described as a perturbation. This suggests that the description of plasmonic eigenmodes in terms of disk eigenmodes provides a viable approach. However, certain features, such as the bowing of the dipole energy, are not properly reproduced by the perturbation results.

In the following we push our perturbation approach even further and allow for additional couplings between disk eigenmodes. The motivation for doing so is provided by the concept of *hybridization* for mixing atomic orbitals into new hybrid orbitals suitable for forming chemical bonds. We first allow for a coupling between the dipole and quadrupole modes by enlarging the matrix of eq 4 to these four states and subsequently diagonalizing the matrix. It is important to realize that mixing of these states, which are orthogonal for the disk, is only possible by the symmetry breaking of F'. The symbols in Figure 3b show that such mixing pushes the dipole energies further down in energy, whereas the quadrupole energies are pushed up. This is reminiscent of ionic bonds in chemistry, where two nondegenerate atomic states couple and become energetically further separated (see sketch shown in inset).

We next allow for couplings between the low-energy hexapole mode and the breathing mode. In a triangular geometry the hexapole mode has opposite charges at the corners and edges and can thus efficiently couple with the breathing mode which has opposite charges at the centers and edges. Indeed, we observe in Figure 3b that the hexapole energy becomes further reduced, as a consequence of this coupling, and the hybridized mode acquires a small component of the breathing mode. This allows us to interpret the transfer of intensity from the breathing mode D to the hexapole mode C observed in Figure 2b in terms of mode hybridization. Altogether, the agreement between the full and the approximate eigenvalues is excellent throughout.

Having established our perturbation and hybridization scheme, we might ask whether the approach also works for different particle geometries. In Figure 4 we show the eigenmode energies and selected eigenfunctions for a silver (a) nanosquare and a (b) nanoellipse. We again observe a nice

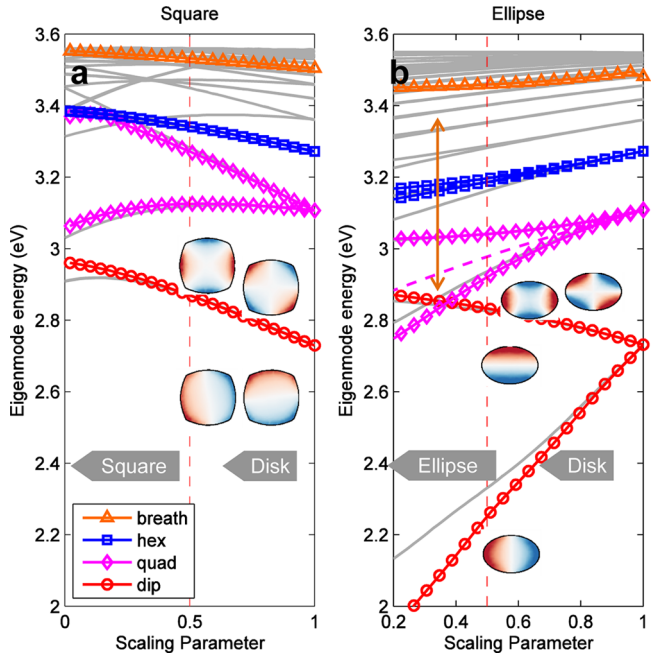

Figure 4. Plasmonic eigenmodes for the silver (a) nanosquare and (b) nanoellipse. For the nanosquare, the perturbation energies are throughout in good agreement with the full results, even without any mode mixing. The insets report the dipole and quadrupole eigenfunctions for a scaling parameter $\xi = 0.5$ (see Methods for definition) indicated by the vertical dashed line. For the nanoellipse shown in panel (b), we allow for a mixing between the quadrupole and breathing modes (results without mixing are shown by the dashed line). The insets report the dipole and quadrupole eigenfunctions for a scaling parameter $\xi = 0.5$ (axis ratio 2:1 for $\xi = 0$).

dx.doi.org/10.1021/nl502027r | Nano Lett. 2014, 14, 4810−4815

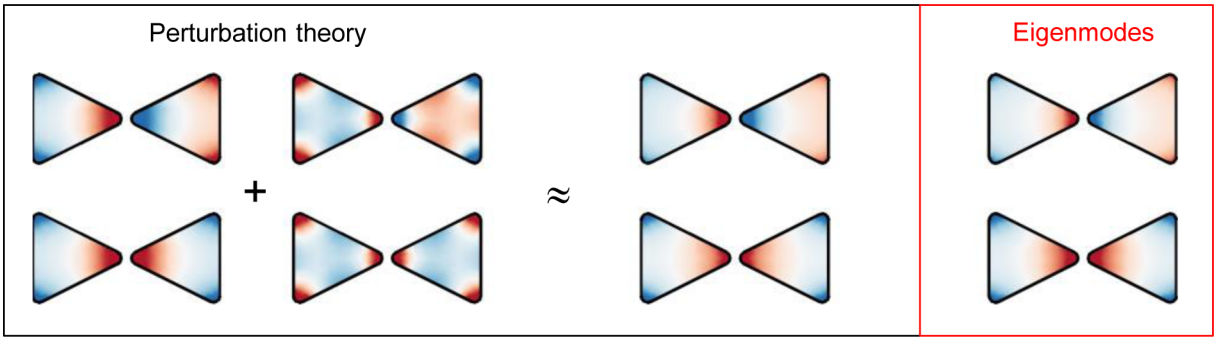

Figure 5. Mode hybridization for a bowtie geometry. The true bonding and antibonding eigenmodes (right panel) with increased surface charges in the hot spot in between the two triangles can be approximately described through a hybridization of the bonding and antibonding dipole and hexapole modes (perturbation theory, left panel).

agreement between the full and the approximate eigenmode energies. For the nanosquare shown in panel (a) the mode energies agree well with the lowest-order approximation of eqs 3 and 4, indicating a minor importance of mode mixing. We also observe a splitting of the quadrupole mode, where the surface charges of the low and high energy part are located at the corners and edges, respectively. For the nanoellipse, the dipole modes split into two modes oriented along the long and short axis, respectively. Also the quadrupole mode undergoes a splitting, and the low-energy mode additionally hybridizes with the breathing mode.

Although the perturbation energies shown in Figures 3 and 4 agree even quantitatively with the true eigenmode energies, we believe that the strength of our approach lies in is its ordering character. It suggests that the disk eigenmodes, which can be naturally characterized in terms of angular order, serve as a basis for the description of SP modes in planar nanoparticles of different geometry. The geometry modification and the corresponding symmetry breaking leads to mode splittings and shifts, as well as to mixing between different modes, such as between film and edge modes. Quite generally, one might employ group theory to find out which modes are allowed to mix for specific symmetries. In this work we have restricted ourselves to sufficiently simple geometries, such that the allowed mixings can be intuitively grasped.

Our perturbation approach can be also combined with the hybridization model for SP modes[6] to describe nanoparticle couplings. As an illustrative example, in Figure 5 we show the coupling between two nanotriangles within a bowtie geometry, leading to the formation of bonding and antibonding modes with parallel and antiparallel dipole moments, respectively. For sufficiently close nanotriangles the surface charges become strongly localized within the gap, giving rise to an additional field enhancement. As schematically shown in the left panel of Figure 5, this modified charge distribution can be described in terms of a hybridization between the dipole and hexapole modes of the nanotriangle.

In comparison to the experimental and simulation results (Figures 1 and 2), based on the solution of the full Maxwell equations, the quasistatic simulations reproduce all essential features but do not quantitatively agree because of the neglect of retardation effects, which lead to significant red shifts of the plasmon resonances. There have recently been strong efforts to extend the concept of plasmonic eigenmodes to "quasinormal modes" within the framework of the full Maxwell equations.[22,23] We believe that our approach could be also extended to such quasinormal modes, which would make our hybridization framework applicable for also larger plasmonic nanoparticles. Alternatively, for sufficiently small nanoparticles one could also employ first- or second-order corrections to the quasistatic approximation.[18]

Methods. In our simulations we use the MNPBEM toolbox,[14] which is based on a boundary element method approach for the solution of Maxwell's equations,[1,11] and its EELS extension.[24] We start with a triangle with rounded edges, as shown at the left top of Figure 1b and extract the triangle contour $r_{tri}(\varphi)$ in polar coordinates. The contour $r(\varphi) = (1 - \xi)r_{tri}(\varphi) + \xi r_{disk}$ is then gradually morphed from the triangle into a disk with radius r_{disk}, using a *scaling* parameter $\xi \in [0,1]$. The diameter of the disk is 300 nm, and the circumference is kept constant for all nanoparticles, in accordance to the nominal values used in experiment, and we discretize the particle boundaries (height 30 nm) using the MNPBEM toolbox routines.[14] As for the dielectric function of silver we use tabulated values extracted from optical experiments.[25] The 15 nm thick SiN membrane is modeled as an additional disk with a radius of 400 nm, using a dielectric constant of $\varepsilon_{SiN} = 4$.

In our computational approach we use during morphing the same particle discretization but only deform the boundary elements, in order to evaluate the matrix elements $F'_{kk'}$ of eq 3 as a simple sum over boundary elements. For too small scaling parameters and for the triangular geometry, some of the boundary elements become too strongly distorted, leading to erroneous results. For this reason we have restricted in Figure 3 the range of scaling parameters to $\xi \geq 0.2$. As for the nanotriangle and nanoellipse shown in Figure 4, the scaling parameter ξ is defined in an analogous way to the triangle.

AUTHOR INFORMATION

Corresponding Author

*E-mail: ulrich.hohenester@uni-graz.at.

Notes

The authors declare no competing financial interest.

ACKNOWLEDGMENTS

This work was supported by the Austria Science Fund (FWF) Projects No. P21800-N20 and P24511-N26, the SFB F49 NextLite, ESTEEM2 (FP7 project, no. 312483), NAWI Graz, and the Graz Centre for Electron Microscopy (ZFE).

REFERENCES

(1) Garcia de Abajo, F. J. *Rev. Mod. Phys.* **2010**, *82*, 209.
(2) Batson, P. E. *Phys. Rev. Lett.* **1982**, *49*, 936.

(3) Bosman, M.; Keast, V. J.; Watanabe, M.; Maaroof, A. I.; Cortie, M. B. *Nanotechnology* **2007**, *18*, 165505.
(4) Nelayah, J.; Kociak, M.; Stephan, O.; Garcia de Abajo, F. J.; Tence, M.; Henrard, L.; Taverna, D.; Pastoriza-Santos, I.; Liz-Martin, L. M.; Colliex, C. *Nat. Phys.* **2007**, *3*, 348.
(5) Kociak, M.; Stephan, O. *Chem. Soc. Rev.* **2014**, *43*, 3865.
(6) Prodan, E.; Radloff, C.; Halas, N. J.; Nordlander, P. *Science* **2003**, *302*, 419.
(7) Nelayah, J.; Kociak, M.; Stephan, O.; Geuquet, N.; Henrard, L.; Garcia de Abajo, F. J.; Pastoriza-Santos, I.; Liz-Marzan, L. M.; Colliex, C. *Nano Lett.* **2010**, *10*, 902.
(8) Gu, L.; Sigle, W.; Koch, C. T.; Ögüt, B.; van Aken, P. A.; Talebi, N.; Vogelgesang, R.; Mu, J.; Wen, X.; Mao, J. *Phys. Rev. B* **2011**, *83*, 195433.
(9) Schmidt, F.-P.; Ditlbacher, H.; Hohenester, U.; Hohenau, A.; Hofer, F.; Krenn, J. R. *Nano Lett.* **2012**, *12*, 5780.
(10) Schmidt, F.-P.; Ditlbacher, H.; Hohenester, U.; Hohenau, A.; Hofer, F.; Krenn, J. R. *Nat. Commun.* **2014**, *5*, 3604.
(11) Garcia de Abajo, F. J.; Howie, A. *Phys. Rev. B* **2002**, *65*, 115418.
(12) Schaffer, B.; Grogger, W.; Kothleitner, G.; Hofer, F. *Ultramicroscopy* **2010**, *110*, 1087.
(13) Brink, H. A.; Barfels, M.; Burgner, R. P.; Edwards, B. N. *Ultramicroscopy* **2003**, *96*, 367.
(14) Hohenester, U.; Trügler, A. *Comput. Phys. Commun.* **2012**, *183*, 370.
(15) Trügler, A.; Tinguely, J.-C.; Jakopic, G.; Hohenester, U.; Krenn, J. R.; Hohenau, A. *Phys. Rev. B* **2014**, *89*, 165409.
(16) Fuchs, R. *Phys. Rev. B* **1975**, *11*, 1732.
(17) Garcia de Abajo, F. J.; Aizpurua, J. *Phys. Rev. B* **1997**, *56*, 15873.
(18) Mayergoyz, I. D.; Fredkin, D. R.; Zhang, Z. *Phys. Rev. B* **2005**, *72*, 155412.
(19) Boudarham, G.; Kociak, M. *Phys. Rev. B* **2012**, *85*, 245447.
(20) Trügler, A.; Tinguely, J. C.; Krenn, J. R.; Hohenau, A.; Hohenester, U. *Phys. Rev. B* **2011**, *83*, 081412(R).
(21) Messiah, A. *Quantum Mechanics*; North-Holland, Amsterdam, 1965.
(22) Kristensen, P. T.; Van Vlack, C.; Hughes, S. *Opt. Lett.* **2012**, *37*, 1649.
(23) Sauvan, C.; Hugonin, J. P.; Maksymov, I. S.; Lalanne, P. *Phys. Rev. Lett.* **2013**, *110*, 237401.
(24) Hohenester, U. *Comput. Phys. Commun.* **2014**, *185*, 1177.
(25) Johnson, P. B.; Christy, R. W. *Phys. Rev. B* **1972**, *6*, 4370.